Supplementary Information

Negligible Increase in Indoor Endotoxin Activity by 222 nm Far-UVC Illumination on Bioaerosols

Zhancong Liang[a], Tim Yiu Cheung[a], Wing Lam Chan[a], Chee Kent Lim[a], Alvin. C.K. Lai[a], Patrick. K.H. Lee[a], Chak K. Chan[a,b]*

[a]*School of Energy and Environment, City University of Hong Kong, 83 Tat Chee Avenue, Kowloon, Hong Kong, China*

[b]*Current address: Current address: Division of Physical Sciences and Engineering, King Abdullah University of Science and Technology, Thuwal, 23955-6900, Saudi Arabia*

*To whom the correspondence should be addressed：
chak.chan@kaust.edu.sa;*chak.k.chan@cityu.edu.hk*.

Content

Text S1. Preparation of the bacteria.

Text S2. Measurements of endotoxin activity.

Text S3. Fraction of membrane-damaged cells.

Text S4. Formation of reactive oxygen species (ROS).

Text S5. Extraction of the bacterial membrane components.

Text S6. Phase transition behaviors and RH-dependent concentrations of KCl particles.

Text S7. Photochemical aging of the bacteria in water suspension and KCl solution.

Text S8. Preparation and photochemical aging of the crystalline matrix containing bacteria.

Figure S1. The schematic of the Teflon chamber system.

Figure S2. Spectra of the far-UVC and UVC light tubes.

Figure S3. Endotoxin activity ratio as a function of time under dark.

Figure S4. The ratio of bound-endotoxin activity in aged cell suspension to the fresh cell suspension.

Text S1. Preparation of the bacteria.

E. coli BW25113 was purchased from the *Coli* Genetic Stock Center (Yale University, USA). Before the experiments, *E. coli* was cultured at 37∘C and 250 rpm for 16 h in LB broth (10 g peptone, 5 g yeast extract, and 10 g NaCl per liter) until cells reached the stationary phase. Cells were then harvested by centrifugation at 13,000× g for 5 min, washed 3 times, and diluted to the target initial colony-forming unit (CFU) per mL by pyrogen-free water or KCl (≥99%, Sigma-Aldrich) solutions. KCl is the major component of saliva, which has phase transition behavior and hygroscopicity similar to artificial saliva [1]. Hence, we used KCl as a surrogate of respiratory fluid and studied the effect of solute concentration on endotoxin release in this study. The optical density (OD) of cells was measured using a cell density meter (Biowave WPA CO 8000, Biochrom Ltd, UK), and a calibration curve was used to convert between OD measurement and CFU/mL.

Text S2. Measurements of endotoxin activity.

The endotoxin activity was determined based on the well-validated Limulus Amebocyte Lysate (LAL) reaction protocol.[2-4] The assay contains a G-factor to eliminate the interference from G-glucan. Specifically, 100 μL Specific LAL assay was well mixed with 100 μL sample and incubated at 37 °C for 8 min to form active proteases. Then, the 100 μL synthetic peptide chromogenic substrate Ac-lle-Glu-Ala-Arg-pNA was added and incubated at 37 °C for 6 min to form pNA. Finally, a diazotization dye: HCl (v/v= 30: 0.4) mixture was added to terminate the reaction and convert the pNA into light-absorbing complexes. The endotoxin activity was determined by the light absorption intensity at 545 nm after calibration using a molecular fluoroscope (SpectraMax M2e). The addition of KCl does not induce low endotoxin recovery (LER) by aggregating the free-endotoxin (Figure S14).[5-7]

By comparing the activity of the free-endotoxin solution before and after filtration, we found that filtration caused some loss of the endotoxin activity, and the recovery depends significantly on the material and slightly on the endotoxin activity. PTFE filtration has the higher recovery (i.e., the smallest loss) of free-endotoxin compared with Nylon and PES (Figure S15). Lower endotoxin activity was found with lower recovery. We developed a relationship between the measured endotoxin activity (i.e., the filtrate) and the actual endotoxin activity (i.e., the unfiltered solution)

(Figure S16). The free-endotoxin activity reported in this study has been scaled using this relationship.

Text S3. Fraction of membrane-damaged cells.

We used the fluorescent dyes propidium iodide (PI, 20 mM in DMSO, Thermo Fisher) and SYBR® Green I (SG, 3.34 mM in DMSO, Thermo Fisher) to measure the fraction of cells with membrane damage. These stains differ in their spectral characteristics and in their ability to penetrate healthy bacterial cells. When used alone, the SG stain generally labels all bacteria in a population — those with intact membranes and those with damaged membranes. In contrast, the PI strain penetrates only bacteria with damaged membranes, causing a reduction in the SG stain fluorescence when both dyes are present. Thus, with an appropriate mixture of the SG and PI stains, bacteria with intact cell membranes stain fluorescent green, whereas bacteria with damaged membranes stain fluorescent red.[8-10]

A 1:1 (v/v) mixture of PI and SG solutions was added to a sterilized centrifuge tube with 2 mL DI water and vigorously vortexed to form a working stain solution. We prepared a new stain solution every time before the measurement. 100 μL of each sample was added to an opaque 96-well microplate (Thermo Fisher) and mixed with 100 μL staining solution. The mixture was then incubated at room temperature and under dark for 15 min. Then, we measured the fluorescence at an excitation wavelength of 485 nm and emission wavelengths of 530 nm (green) and 630 nm (red), using a molecular fluoroscope (SpectraMax M2e).[11, 12] The fluorescent intensity ratio of red to green was used to determine the fraction of membrane-damaged cells, based on calibration using alive and dead cell mixtures in known ratios. The dead cell was prepared by heating the cell suspension at 90 °C for 15 min, then mixed with the alive cell suspension after cooling down to the temperature. The background remains virtually nonfluorescent.

Text S4. Formation of reactive oxygen species (ROS).

The intracellular ROS was measured by 2',7'-dichlorodihydrofluorescein diacetate (H2DCFDA, ≥97%, Sigma), which is a chemically reduced form of fluorescein. Upon oxidative cleavage of the

acetate groups by ROS, the nonfluorescent H2DCFDA is converted to the highly fluorescent 2',7'-dichlorofluorescein (DCF). The fluorescent intensity of DCF indicated the amount of ROS.[13]

1mL cell suspension was centrifuged at 13000× g for 5 min at room temperature, and the supernatant was removed. 1mL 5 µM H2DCFDA in sterilized and filtrated water was mixed with the cell pellet and incubated at 37 °C for 1 hour. Then, the mixture was centrifuged again, and after the supernatant was removed. The cell pellet was washed 3 times using phosphate-buffered saline (PBS) to remove the extracellular H2DCFDA. Afterward, the cell pellet was resuspended in 1mL PBS. Finally, the fluorescence at 488nm/525nm excitation/emission of the cell suspension was measured using a molecular fluoroscope (SpectraMax M2e).[14] We measured the ROS formation in the membrane suspension separated from cells, using the same protocol as used for intact cell suspension.

Text S5. Extraction of the bacterial membrane components.

The cells were disrupted using an ultrasonic cell disruptor (LICHEN) for 2 min. The cell suspension was conditioned in an ice bath to avoid unwanted damage to cellular components by heat during ultrasonic treatment. The fraction of membrane-damage cells after the 2 min disruption was close to 1, based on the PI/SG staining method introduced above. After the disruption, we centrifuged the cell suspension at 10000 rpm for 5 min. The supernatant was removed, and the pellet was resuspended using pyrogen-free solutions, denoted as the membrane components. We found the DCF fluorescence intensity from membrane component separated at 10000 rpm became similar to that of the intact cell and insensitive to the further rotational speed increase, by illuminating both using 222 nm for 2 min (Figure S17). Then we assumed 10000 rpm was sufficient for membrane separation.

Text S6. Phase transition behaviors and RH-dependent concentrations of KCl particles.

We examined the phase transition of deposited KCl droplets (on a hydrophobic substrate) with different concentrations of cells using a flow-cell system coupled with a microscope (Figure S5). The morphological change from spheric droplets to irregularly shaped solids suggests that

efflorescence has taken place.[1, 15] The efflorescence RH (ERH) of KCl particles was found at around 50%, (consistent with the literature[16, 17], irrespective of the cell concentration in the range of 10^5-10^7 CFU/mL (Figure S9).

Assuming spherical particles, the concentration of the KCl were calculated based on the measurements of the growth factor (GF, the volume ratio of an equilibrated wet particles to the dry particle) (Equation 1), using a microscope-flow cell system demonstrated in our previous work.[1]

$$[KCl] = \frac{m_{KCl}}{V_{Wet}} = \frac{V_{KCl} \times \rho_{KCl}}{V_{Wet}} = \frac{\rho_{KCl}}{GF}$$

(1)

where m_{KCl} is the mass of the KCl, $V_{KCl,}$ and V_{Wet} are the volume of the KCl and wet droplet, respectively. ρ_{KCl} is the density of the KCl (1984 g/L). The [KCl] concentration as a function of RH from 50% to 93% is shown in Figure S6. Since RH higher than 93% was not accessible due to experimental limitation, we extrapolated the fitting curve ($R^2 = 0.9985$) to calculate the concentration.

**Text S7.** Photochemical aging of the bacteria in water suspension and KCl solution.

A 200 μL cell suspension and a cell-free solution (KCl or water) were added to two quartz cuvettes, respectively. The cell-free solution controls any endotoxin from the illuminated solution or ambient. A number of 222 nm KrCl* excimer (30W, DM222, Daylight) or 254 nm Hg (30W, TUV, Philip) light tubes were installed above the cuvettes (Figure S7). The irradiation distance of the 254 nm light tube was adjusted to make the light intensity comparable with the 222 nm light tubes (~550 μW/cm^2). The depth of the suspension was around 1 cm. A bladeless fan was used to cool the light tube when it was on. The temperature was maintained at 21±0.4 °C as measured by a status scope (SCIEX). The mass change of the suspension was less than 0.01% after 10 min. Thus, we considered the uncertainty induced by evaporation negligible.

Text S8. The effect of crystallization on the EA increase rate constant.

We carried out additional experiments to explore the effect of crystallization on the EA increase rate constant. The 1 μL bacteria-containing droplets were deposited onto a hydrophobic substrate in a flow cell and dried by filter-sterilized synthetic air until they formed solid particles, as observed under the microscope (Figure S5). Then, we adjusted the RH using a wet-dry mixed flow to the desired level and illuminated the particles. After illumination, the hydrophobic substrate was moved to an endotoxin-specific storage tube (Bioendo) with 1 mL pyrogen-free water and vigorously vortexed for 2 min. The recovery of free-endotoxin in KCl crystalline particles using this method reached (96±3.3) %. The calculation of the EA increase rate constant for these particles was the same as that used for cuvette samples. The transmission of the quartz window of the flow cell at 222 nm is around 70%. Thus we multiplied the incident UV doses by 0.7 when calculating the EA increase rate constant of flow cell samples.[15]
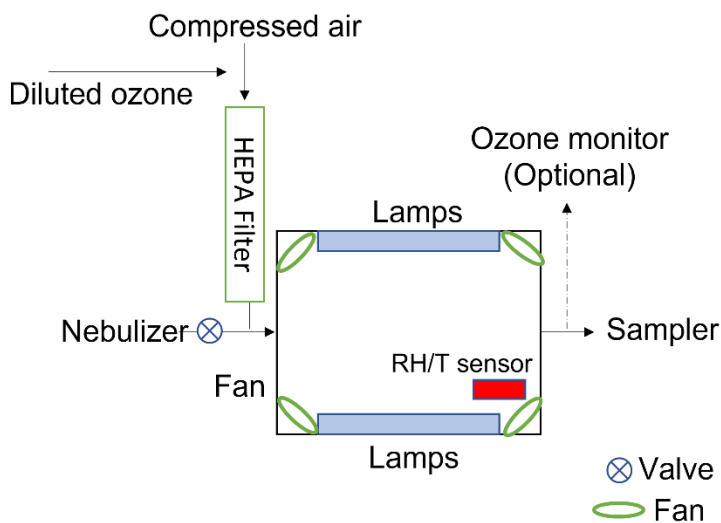
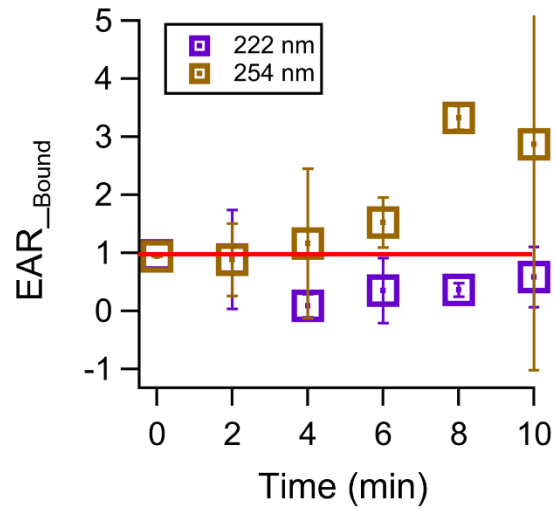**Figure S1.** The schematic of the Teflon chamber system.
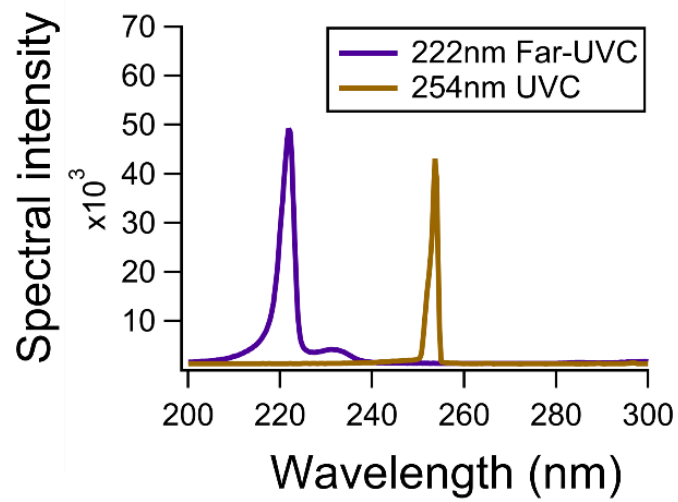
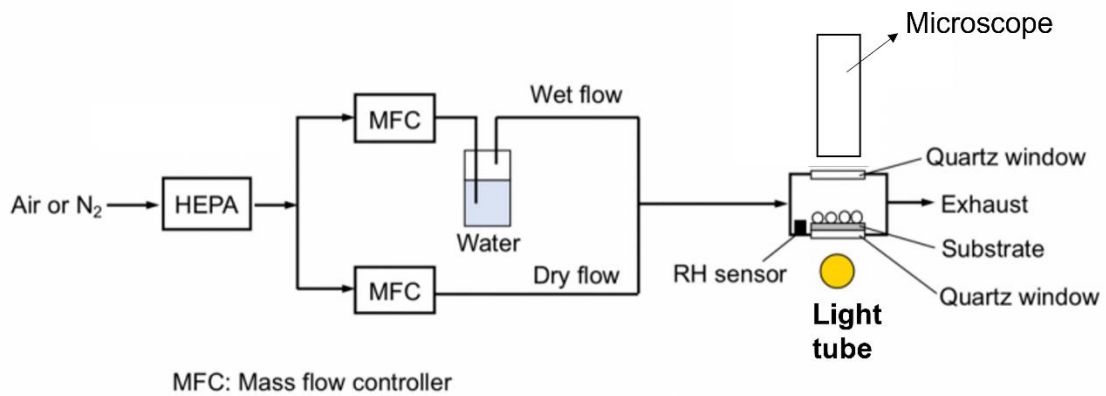**Figure S2.** Spectra of the far-UVC and UVC light tubes.
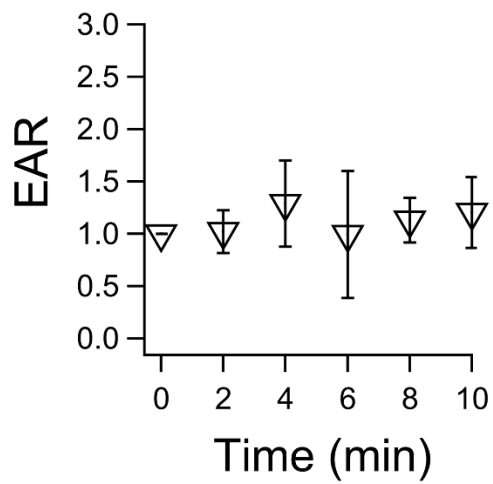
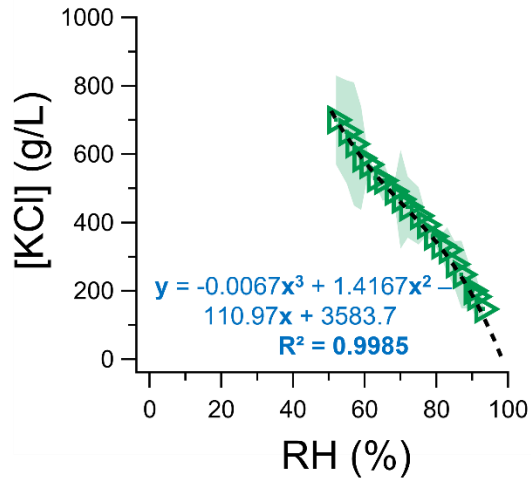**Figure S3.** Endotoxin activity ratio as a function of time under dark.

Figure S4. The ratio of bound-endotoxin activity in aged cell suspension to the fresh cell suspension. The red solid line denotes endotoxin activity ratio of 1.

Figure S5. Experimental schematic of the flow-cell system. A detailed description of the set-up can be found in [1, 15].

Figure S6. The Concentration of KCl in aqueous droplets as a function of RH. The shaded area shows the standard derivation.
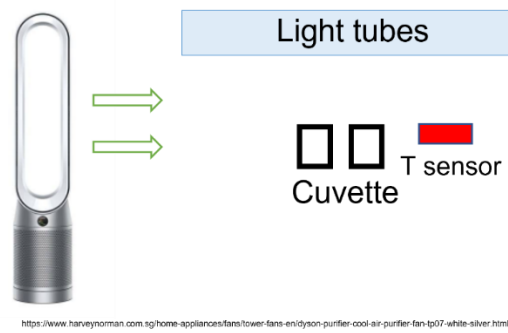
Figure S7. Experimental schematic of photo illumination of cell suspensions.
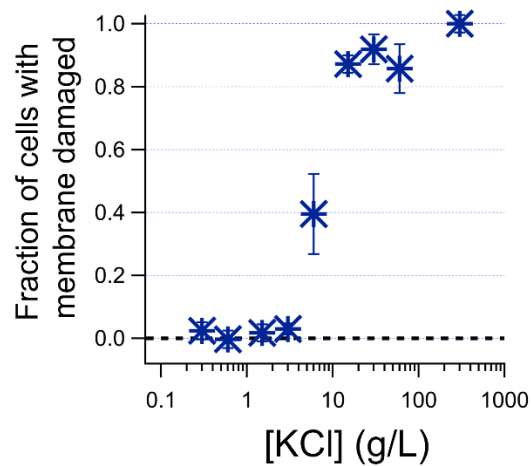
Figure S8. Fraction of membrane-damaged cells at different [KCl]. The black dashed line shows the average result at [KCl] = 0 g/L.
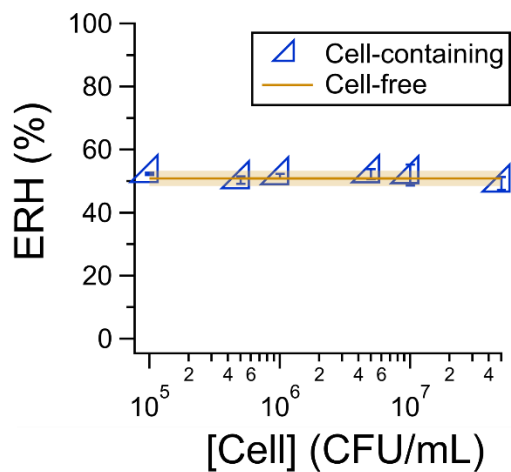
Figure S9. ERH of KCl particles as a function of cell concentration.
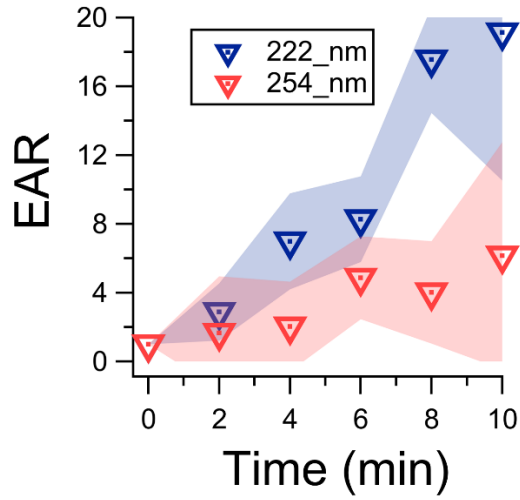
Figure S10. EAR as a function of time of *Pseudomonas putida* suspension in pyrogen-free DI water. The bacteria were grown at 25∘C and 250 rpm for 16 h in nutrient broth (NB).
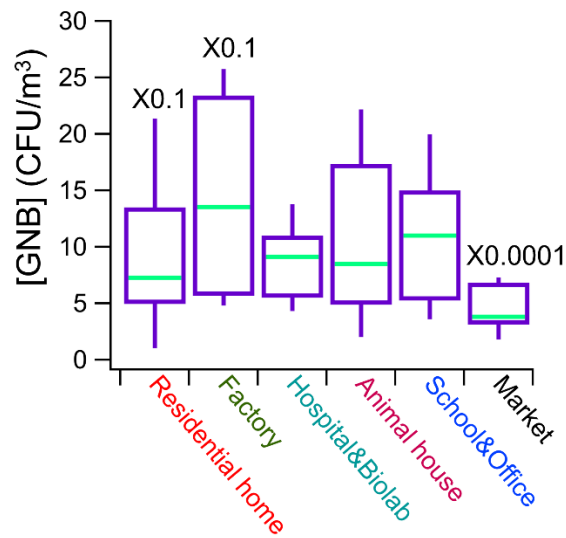
Figure S11. Reported concentration of gram-negative bacteria in different indoor areas.[18-32]
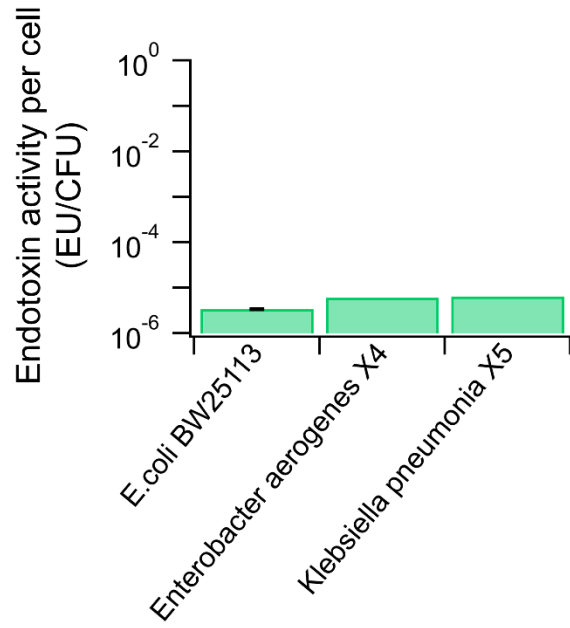
Figure S12. The endotoxin activity per culturable gram-negative bacteria. The results of Enterobacter aerogenes X4 and Klebsiella pneumonia X5 are from Xue et al. (2019).[33]
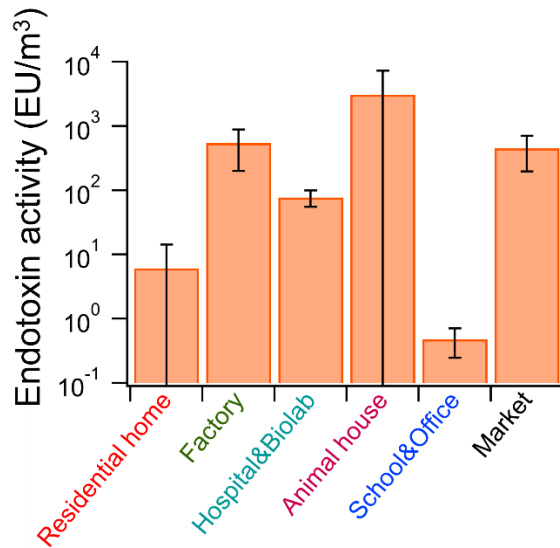
Figure S13. Reported endotoxin activity in different indoor areas.[19, 34-46]
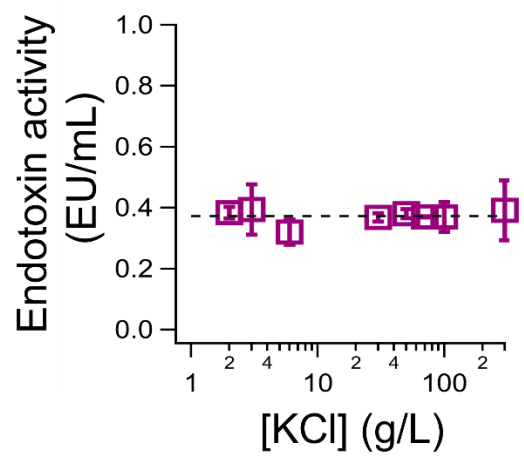
Figure S14. Endotoxin activity as a function of KCl concentration.
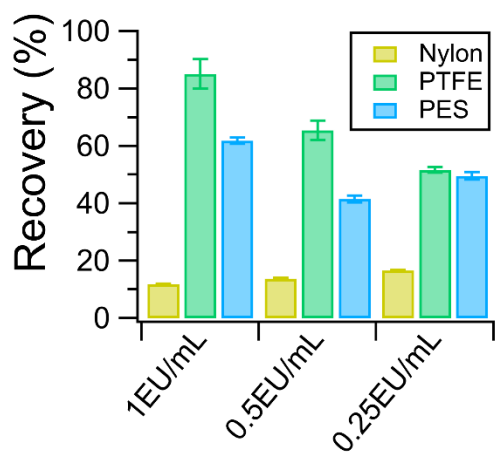
Figure S15. Recovery of endotoxin activity in filtration using different filters.
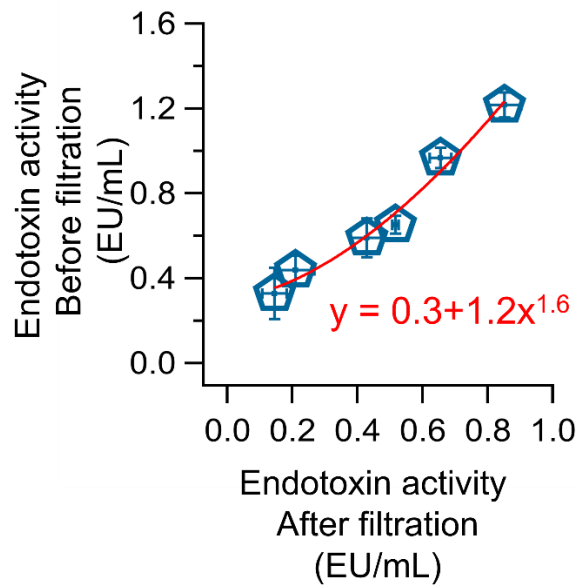
Figure S16. Endotoxin activity after filtration as a function of endotoxin activity before filtration.
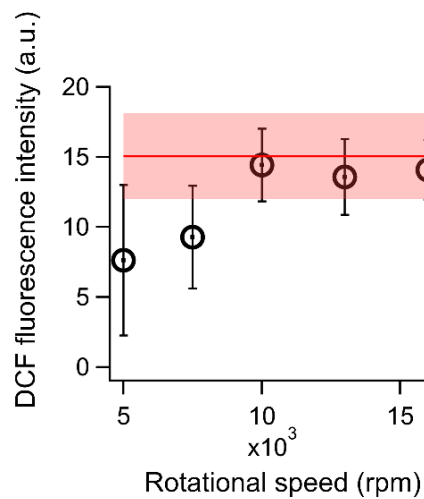
Figure S17. The DCF fluorescence intensity of membrane-component after 2 min of 222 nm illumination as a function of rotational speed for membrane separation. The red region indicates the DCF fluorescence intensity of 222 nm illuminated intact cell for 2 min.

Table S1. The summarized EA increase rate constants at different conditions.

[KCl] (g/L)	[Cell] (CFU/mL)	Equivalent RH (%)	EA increase rate constant $\times 0.1$ (UV dose^{-1})
300	1.50E+07	83.1	(5.48 ± 1.01)
100	5.00E+06	94.2	(5.31 ± 0.72)
70	3.50E+06	95.6	(4.58 ± 0.64)
50	2.50E+06	96.4	(4.17 ± 0.81)
30	1.50E+06	97.2	(4.42 ± 0.87)
6	3.00E+05	98.1	(4.29 ± 0.39)
3	1.50E+05	98.2	(4.67 ± 0.63)
2	1.00E+05	98.3	(5.17 ± 1.17)
300	1.00E+05	83.1	(5.76 ± 1.48)
100	1.00E+05	94.2	(5.16 ± 0.42)
200	1.00E+07	89.3	(4.62 ± 1.20)
395	1.98E+07	75.7	(5.32 ± 0.13)
458	2.29E+07	70.1	(5.97 ± 0.72)
523	2.62E+07	64.4	(4.60 ± 1.31)
572	2.86E+07	60.5	(6.30 ± 0.12)
661	3.30E+07	54.4	(5.81 ± 0.46)
N.A.	N.A.	40.0	(0.90 ± 0.04)
N.A.	N.A.	20.0	(0.48 ± 0.07)
N.A.	N.A.	5.0	(0.67 ± 0.03)
N.A.	N.A.	40.9	(0.18 ± 0.14)[a]
N.A.	N.A.	23.2	(0.08 ± 0.09)[a]
N.A.	N.A.	5.7	(0.12 ± 0.07)[a]

[a] Data from the flow-cell experiments.

Reference

(1) Liang, Z.; Chan, W. L.; Tian, X.; Lai, A. C. K.; Lee, P. K. H.; Chan, C. K. Inactivation of Escherichia coli in droplets at different ambient relative humidities: Effects of phase transition, solute and cell concentrations. *Atmospheric Environment* **2022**, *280*, 119066. DOI: https://doi.org/10.1016/j.atmosenv.2022.119066.

(2) Huang, H.; Wu, Q.-Y.; Yang, Y.; Hu, H.-Y. Effect of chlorination on endotoxin activities in secondary sewage effluent and typical Gram-negative bacteria. *Water Research* **2011**, *45* (16), 4751-4757. DOI: https://doi.org/10.1016/j.watres.2011.06.013.

(3) Ding, H.; Zhu, Z.; Tang, T.; Yu, D.; Yu, B.; Dai, K. Comparison of the cytotoxic and inflammatory responses of titanium particles with different methods for endotoxin removal in RAW264. 7 macrophages. *Journal of Materials Science: Materials in Medicine* **2012**, *23* (4), 1055-1062.

(4) Liu, Y.; Tang, Q.; Zhang, J.; Xia, Y.; Yang, Y.; Wu, D.; Fan, H.; Cui, S. W. Triple helix conformation of β-d-glucan from Ganoderma lucidum and effect of molecular weight on its immunostimulatory activity. *International journal of biological macromolecules* **2018**, *114*, 1064-1070.

(5) Cao, Y.; Zhang, Y.; Qiu, F. Low endotoxin recovery and its impact on endotoxin detection. *Biopolymers* **2021**, *112* (11), e23470.

(6) Tsuchiya, M. Factors affecting reduction of reference endotoxin standard activity caused by chelating agent/detergent matrices: Kinetic analysis of low endotoxin recovery. *PDA Journal of Pharmaceutical Science and Technology* **2017**, *71* (6), 478-487.

(7) Reich, J.; Weyer, F. A.; Tamura, H.; Nagaoka, I.; Motschmann, H. Low endotoxin recovery—Masking of naturally occurring endotoxin. *International journal of molecular sciences* **2019**, *20* (4), 838.

(8) Nescerecka, A.; Hammes, F.; Juhna, T. A pipeline for developing and testing staining protocols for flow cytometry, demonstrated with SYBR Green I and propidium iodide viability staining. *Journal of microbiological methods* **2016**, *131*, 172-180.

(9) Bensch, G.; Rüger, M.; Wassermann, M.; Weinholz, S.; Reichl, U.; Cordes, C. Flow cytometric viability assessment of lactic acid bacteria starter cultures produced by fluidized bed drying. *Applied microbiology and biotechnology* **2014**, *98* (11), 4897-4909.

(10) Liang, L.; Wu, L.; Xu, W.; Liu, C.; Liu, X.; Cheng, H.; Liu, Y.; Zhang, G.; Che, H.; Sun, J. The characterization and quantification of viable and dead airborne biological particles using flow cytometry and double fluorescent staining. *Journal of Aerosol Science* **2022**, 106019.

(11) Feng, J.; Yee, R.; Zhang, S.; Tian, L.; Shi, W.; Zhang, W.-H.; Zhang, Y. A rapid growth-independent antibiotic resistance detection test by SYBR green/propidium iodide viability assay. *Frontiers in medicine* **2018**, *5*, 127.

(12) Robertson, J.; McGoverin, C.; Vanholsbeeck, F.; Swift, S. Optimisation of the protocol for the LIVE/DEAD® BacLightTM bacterial viability kit for rapid determination of bacterial load. *Frontiers in microbiology* **2019**, *10*, 801.

(13) Szychowski, K. A.; Rybczyńska-Tkaczyk, K.; Leja, M. L.; Wójtowicz, A. K.; Gmiński, J. Tetrabromobisphenol A (TBBPA)-stimulated reactive oxygen species (ROS) production in cell-free model using the 2′, 7′-dichlorodihydrofluorescein diacetate (H2DCFDA) assay—limitations of method. *Environmental Science and Pollution Research* **2016**, *23* (12), 12246-12252.

(14) Chompoosor, A.; Saha, K.; Ghosh, P. S.; Macarthy, D. J.; Miranda, O. R.; Zhu, Z. J.; Arcaro, K. F.; Rotello, V. M. The role of surface functionality on acute cytotoxicity, ROS generation and DNA damage by cationic gold nanoparticles. *Small* **2010**, *6* (20), 2246-2249.

(15) Liang, Z.; Zhang, R.; Gen, M.; Chu, Y.; Chan, C. K. Nitrate Photolysis in Mixed Sucrose–Nitrate–Sulfate Particles at Different Relative Humidities. *The Journal of Physical Chemistry A* **2021**, *125* (17), 3739-3747. DOI: 10.1021/acs.jpca.1c00669.

(16) Jing, B.; Peng, C.; Wang, Y.; Liu, Q.; Tong, S.; Zhang, Y.; Ge, M. Hygroscopic properties of potassium chloride and its internal mixtures with organic compounds relevant to biomass burning aerosol particles. *Scientific reports* **2017**, *7* (1), 1-11.

(17) Li, X.; Gupta, D.; Eom, H.-J.; Kim, H.; Ro, C.-U. Deliquescence and efflorescence behavior of individual NaCl and KCl mixture aerosol particles. *Atmospheric Environment* **2014**, *82*, 36-43.

(18) Adhikari, A.; Kettleson, E. M.; Vesper, S.; Kumar, S.; Popham, D. L.; Schaffer, C.; Indugula, R.; Chatterjee, K.; Allam, K. K.; Grinshpun, S. A.; Reponen, T. Dustborne and airborne Gram-positive and Gram-negative bacteria in high versus low ERMI homes. *Science of The Total Environment* **2014**, *482-483*, 92-99. DOI: https://doi.org/10.1016/j.scitotenv.2014.02.110.

(19) Balasubramanian, R.; Nainar, P.; Rajasekar, A. Airborne bacteria, fungi, and endotoxin levels in residential microenvironments: a case study. *Aerobiologia* **2012**, *28* (3), 375-390. DOI: 10.1007/s10453-011-9242-y.

(20) Fang, Z.; Gong, C.; Ouyang, Z.; Liu, P.; Sun, L.; Wang, X. Characteristic and Concentration Distribution of Culturable Airborne Bacteria in Residential Environments in Beijing, China. *Aerosol and Air Quality Research* **2014**, *14* (3), 943-953. DOI: 10.4209/aaqr.2013.04.0109.

(21) Prazmo, Z.; Dutkiewicz, J.; Skorska, C.; Sitkowska, J.; Cholewa, G. Exposure to airborne Gram-negative bacteria, dust and endotoxin in paper factories. *Annals of Agricultural and Environmental Medicine* **2003**, *10* (1).

(22) Park, D.-U.; Yeom, J.-K.; Lee, W. J.; Lee, K.-M. Assessment of the levels of airborne bacteria, gram-negative bacteria, and fungi in hospital lobbies. *International journal of environmental research and public health* **2013**, *10* (2), 541-555.

(23) Hwang, S. H.; Lee, I. M.; Yoon, C. S. Levels of total airborne bacteria, gram-negative bacteria, and endotoxin according to biosafety levels in Korean biosafety laboratories. *Human and Ecological Risk Assessment: An International Journal* **2013**, *19* (6), 1576-1585.

(24) Nasir, Z. A.; Mula, V.; Stokoe, J.; Colbeck, I.; Loeffler, M. Evaluation of total concentration and size distribution of bacterial and fungal aerosol in healthcare built environments. *Indoor and Built Environment* **2015**, *24* (2), 269-279.

(25) Mirhoseini, S. H.; Didehdar, M.; Akbari, M.; Moradzadeh, R.; Jamshidi, R.; Torabi, S. Indoor exposure to airborne bacteria and fungi in sensitive wards of an academic pediatric hospital. *Aerobiologia* **2020**, *36* (2), 225-232.

(26) Zucker, B. A.; Trojan, S.; Müller, W. Airborne gram-negative bacterial flora in animal houses. *Journal of Veterinary Medicine, Series B* **2000**, *47* (1), 37-46.

(27) Chang, C.; Chung, H.; Huang, C.-F.; Su, H.-J. J. Exposure of workers to airborne microorganisms in open-air swine houses. *Applied and Environmental Microbiology* **2001**, *67* (1), 155-161.

(28) Dutkiewicz, J.; Pomorski, Z. J.; Sitkowska, J.; Krysińska-Traczyk, E.; Skórska, C.; Prażmo, Z.; Cholewa, G.; Wójtowicz, H. Airborne microorganisms and endotoxin in animal houses. *Grana* **1994**, *33* (2), 85-90.

(29) Aydogdu, H.; Asan, A.; Tatman Otkun, M. Indoor and outdoor airborne bacteria in child day-care centers in Edirne City (Turkey), seasonal distribution and influence of meteorological factors. *Environmental monitoring and assessment* **2010**, *164* (1), 53-66.

(30) Tsai, F.; Macher, J.; Hung, Y. Concentrations of airborne bacteria in 100 US office buildings. *Proceedings of Indoor Air* **2002**, *4*, 353-358.

(31) Tsai, F.; Macher, J. Concentrations of airborne culturable bacteria in 100 large US office buildings from the BASE study. *Indoor air* **2005**, *15* (9), 71-81.

(32) Reanprayoon, P.; Yoonaiwong, W. Airborne concentrations of bacteria and fungi in Thailand border market. *Aerobiologia* **2012**, *28* (1), 49-60.

(33) Xue, J.; Zhang, J.; Qiao, J.; Lu, Y. Effects of chlorination and combined UV/Cl2 treatment on endotoxin activity and inhalation toxicity of lipopolysaccharide, gram-negative bacteria and reclaimed water. *Water Research* **2019**, *155*, 124-130. DOI: https://doi.org/10.1016/j.watres.2019.02.021.

(34) Niu, M.; Shen, F.; Zhou, F.; Zhu, T.; Zheng, Y.; Yang, Y.; Sun, Y.; Li, X.; Wu, Y.; Fu, P.; Tao, S. Indoor air filtration could lead to increased airborne endotoxin levels. *Environment International* **2020**, *142*, 105878. DOI: https://doi.org/10.1016/j.envint.2020.105878.

(35) Yen, Y.-C.; Yang, C.-Y.; Wang, T.-N.; Yen, P.-C.; Ho, C.-K.; Mena, K. D.; Lee, T.-C.; Chen, K.-S.; Lin, Y.-C.; Chen, P.-S. Household airborne endotoxin associated with asthma and allergy in elementary school-age children: a case–control study in Kaohsiung, Taiwan. *Environmental Science and Pollution Research* **2020**, *27* (16), 19502-19509.

(36) Yen, Y.-C.; Yang, C.-Y.; Ho, C.-K.; Yen, P.-C.; Cheng, Y.-T.; Mena, K. D.; Lee, T.-C.; Chen, P.-S. Indoor ozone and particulate matter modify the association between airborne endotoxin and schoolchildren's lung function. *Science of the Total Environment* **2020**, *705*, 135810.

(37) Tefera, Y.; Schlünssen, V.; Kumie, A.; Deressa, W.; Moen, B. E.; Bråtveit, M. Personal inhalable dust and endotoxin exposure among workers in an integrated textile factory. *Archives of Environmental & Occupational Health* **2020**, *75* (7), 415-421.

(38) Asgedom, A. A.; Bråtveit, M.; Schlünssen, V.; Moen, B. E. Exposure to inhalable dust, endotoxin and formaldehyde in factories processing particleboards from eucalyptus trees in Ethiopia. *Environmental and Occupational Health Practice* **2020**, *2* (1), 2019-0016-OA.

(39) Tefera Zele, Y.; Kumie, A.; Deressa, W.; Moen, B. E.; Bråtveit, M. Reduced cross-shift lung function and respiratory symptoms among integrated textile factory workers in Ethiopia. *International journal of environmental research and public health* **2020**, *17* (8), 2741.

(40) Liu, H.; Zhang, Z.; Wen, N.; Wang, C. Determination and risk assessment of airborne endotoxin concentrations in a university campus. *Journal of Aerosol Science* **2018**, *115*, 146-157.

(41) Di Renzi, S.; Chiominto, A.; Marcelloni, A. M.; Melis, P.; Riviello, M. C.; Wirz, A.; Sisto, R.; Massari, S.; Paba, E.; D'ovidio, M. C. Work Category Affects the Exposure to Allergens and Endotoxins in an Animal Facility Laboratory in Italy: A Personal Air Monitoring Study. *Applied Sciences* **2021**, *11* (16), 7220.

(42) Madsen, A. M.; White, J. K.; Nielsen, J. L.; Keskin, M. E.; Tendal, K.; Frederiksen, M. W. A cross sectional study on airborne inhalable microorganisms, endotoxin, and particles in pigeon coops–Risk assessment of exposure. *Environmental Research* **2022**, *204*, 112404.

(43) Pilote, J.; Létourneau, V.; Girard, M.; Duchaine, C. Quantification of airborne dust, endotoxins, human pathogens and antibiotic and metal resistance genes in Eastern Canadian swine confinement buildings. *Aerobiologia* **2019**, *35* (2), 283-296.

(44) Shin, S.-J.; Song, E.-S.; Kim, J.-W.; Lee, J.-H.; Gautam, R.; Kim, H.-J.; Kim, Y.-G.; Cho, A.-R.; Yang, S.-J.; Acharya, M. Major environmental characteristics of swine husbandry that affect exposure to dust and airborne endotoxins. *Journal of Toxicology and Environmental Health, Part A* **2019**, *82* (4), 233-243.

(45) Hwang, S.; Kim, S.-Y.; Choi, S.; Lee, S.; Park, D.-U. Correlation between levels of airborne endotoxin and heavy metals in subway environments in South Korea. *Scientific Reports* **2021**, *11* (1), 1-8.
(46) Wei, D.-J.; Liu, W.-T.; Chin, H.-T.; Lin, C.-H.; Chen, I.-C.; Chang, Y.-T. An investigation of airborne bioaerosols and endotoxins present in indoor traditional wet markets before and after operation in Taiwan: A case study. *International journal of environmental research and public health* **2021**, *18* (6), 2945.